UNIVERSITY OF PADUA

ICEA DEPARTMENT

MASTER SCIENCE DEGREE

IN ENVIRONMENTAL ENGINEERING

An experimental investigation on the trajectories of floating particles captured because of Cheerios Effect by a cylindrical collector

SUPERVISOR:

Prof. Andrea Defina

ASSISTANT SUPERVISOR:

Ing. Paolo Peruzzo

STUDENT:

Andrea Schiavon

A.Y. 2013/2014

Ai miei genitori

CONTENTS

INTRODUCTION

In natural rivers the seeds of many plants or organic particles keep afloat and for this reason they are transported on the water surface. Close to emergent vegetation, these seeds and particles are subjected to the surface tension that may enhance their retention in proximity of emergent plants.

For the floating particles, a mechanism of capture is a direct interception where the trapping is due to a direct contact; however this process cannot describe completely the capture of buoyancy particles. The surface tension, to which the particles are subjected to, causes a surface deformation and the formation of capillary forces whose effects cannot be neglected.

For what said above the Cheerios effect, i.e. the clustering of floating bodies on water surface, plays a fundamental role on the mechanisms of capture and retention of partially emergent vegetation in wetlands. Despite of the importance of capillary capture in flowing fluid, few physically based or experimental works currently exist for this process.

This thesis analyses the trapping mechanisms of spherical particles with different diameters close to cylindrical collectors with vertical axis and subjected to uniform flows.

The experimental investigations were carried out in an artificial channel of the Hydraulic laboratory at the University of Padua. To simulate the interaction process between emerging vegetation and floating seeds were used wooden vertical cylinders and some floating PCE spheres. Recorded trajectories were then compared with numerical trajectories predicted by a numerical model (*Peruzzo et al.*; 2013).

The aim of this thesis is to verify if the numerical model gives a good description of the observed phenomena.

In the following part it is summarized the content of every chapter.

Chapter one describes the theoretical aspects involved in the trapping mechanism; a particular relevance is given to the surface tension and to the development of the numerical model of *Peruzzo et al.*.

Chapter two deals with the methods used to carry on laboratory tests and to fix same data. After a description of the channel and its functioning there is the explanation of two main points: the procedure to create a uniform flow and the statistics to assign the velocities. The values obtained are reported in the last part.

Chapter three : after the elaboration of the data from the camera and, more generally, from the laboratory, the trajectories have been recreated. The obtained results have been compared with those of the numerical model of *Peruzzo et al.*.

1 THEORETICAL ASPECTS

This chapter is focused on the main aspects that can be involved in uniform condition in the trapping of a floating particle in the vicinity of a vertical cylinder, and in the deviating of particle from its original path. It describes the mechanisms of the attraction and explains the numerical model used to represent all these aspects.

1.1 The interaction mechanisms

When a particle interacts with a cylinder it is affected by an attraction force towards the cylinder and it can change its original trajectory or being trapped by the collector. These processes are due to some mechanisms as *i)* the inertial impaction, *ii)* the wake trapping and *iii)* the surface tension through the Cheerios effect. The latter is particularly relevant so a detailed description will be developed.

The inertial impaction occurs when a particle deviates from its streamline because of its inertia and collides with the cylinder (*Defina & Peruzzo*; 2010). Generally, after the impact, the particle moves around the cylinder. Sometimes It is not easy to distinguish this mechanism from that which involves the surface tension because of the same paths followed by the particle.

The wake trapping can be observed when a particle enters into unsteady recirculation zone behind a collector following an irregular path. It must be noted that the weak region formed behind a cylinder rather than the particle trapping, enhances a particle dispersion due to the randomly velocity field created (*White & Nepf*; 2003) . The effectiveness of the wake trapping is strictly related with the vortex shedding model. For certain values of the Reynolds number *Re*, the formation of vortices can occur in this wake zone. Considering very small values of *Re*, the flow is symmetric fore and aft of the cylinder, indeed, it looks not only steady but very stable (fig. 2.1a) (*Drazin*; 2002).

When *Re* increases to about 10, the flow has been visibly separated in order to form a pair of recirculating eddies in the backside of the cylinder. As *Re* increases

further, the lines of separation move upstream and the eddies grow longer as a wake, but the flow remains steady and retains its symmetry (fig. 2.1b) (*Drazin*; 2002).

As *Re* reaches values near to 48, the flow becomes unsteady and the eddies begin to oscillate. For Re>48 vortex shedding appears, i.e. the vortices are alternatively detached from the separated streamlines above and below the cylinder (fig. 2.1c).

For *Re* higher than 1300, the length of vortex formation starts to shrink; instead, for *Re* values higher than $2 \cdot 10^5$ the vortex shedding does not occur in an alternating, but the wake is characterized by disordered eddies (fig. 2.1d). This presence modifies the velocity of the flow and the lateral force in the cylinder (*Drazin*, 2002). These aspects are the reason why particles trajectories can be different in departing from the cylinder.

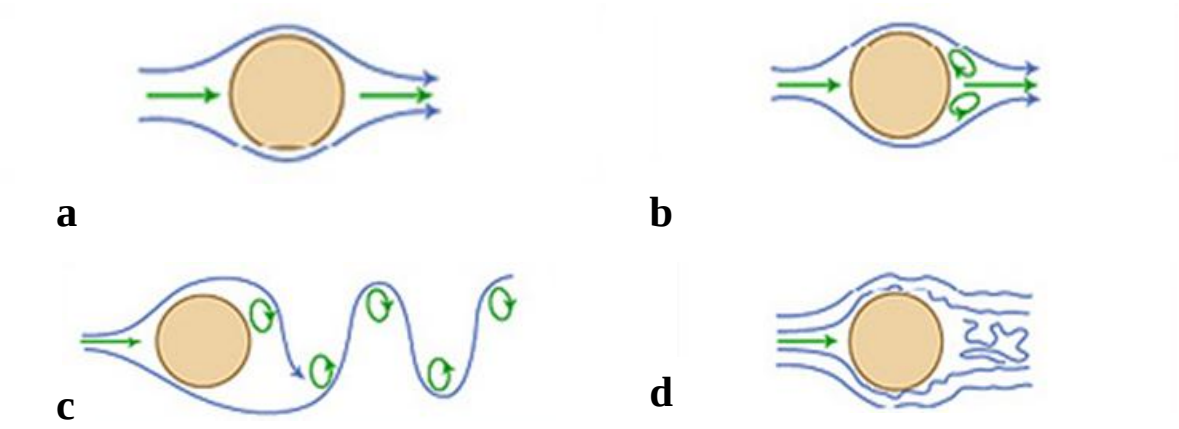

Fig 1.1: The wake zone: (a) Creeping Flow Re < 10, (b) Attached vortices $10 < Re < 48$, (c) Von Karman vortex trail $40 < Re < 200.000$, (d) Fully turbulent wake, Re > 200.000

The vortex shedding frequency f can be determined with the Strouhal number Sr, that depends directly on the *Re*.

From the beginning of the vortex shedding up to the laminar-turbulent transition of the cylinder boundary layer at $Re > 2 \times 10^5$, the relation between Strouhal number: $Sr = f d_c / U$ and Reynolds number: $Re = U d_c / \nu$ where U is the incoming flow velocity. d_c the cylinder diameter, ν the kinematic viscosity of the fluid and f is the shedding frequency. If Sr is function of $1/\sqrt{Re}$ a relationship exits given by $Sr = Sr^* + m/\sqrt{Re}$ (*Fey et al.*, 1998).

The coefficients Sr^* and m assume different tabulated values as function of Re number (*Fey et al.*, 1998).

***Tab1.1**: Coefficients Sr^* and m as function of Re range regarding this thesis*

Re	Sr^*	m
$47 < Re < 180$	0.2684	-1.0356
$180 < Re < 230$	0.2437	-0.8607
$230 < Re < 240$	0.4291	-3.6735
$240 < Re < 360$	*Depends on boundary condition*	
$360 < Re < 1300$	0.2257	-0.4402

In the regular range $47 < Re < 180$ Sr is function of Re by a linear relationship. Also for $Re > 180$ the Strouhal-Reynolds dependency is represented by piecewise linear relationships.

In the interval $240 < Re < 360$ the Strouhal number is highly dependent on the boundary condition of the cylinder; hence, here no generally valid relation can be given.

1.2 The Cheerios effect

Molecular forces act in interfaces between two immiscible liquids, such as in the case of this thesis, between a liquid (i.e. water) and gas (i.e. air). The resulting force, for unit length, is defined superficial tension σ.

As a consequence, the formation of a rising curvature of liquid surface can be observed in proximity of the channel walls or emerging cylinders. It is named meniscus (fig. 2.2). The angle ψ that the separation surface creates, depends on tensions generated between water-air, water-solid and solid-air, and the nature of the materials in contact.

The Cheerios effect can be described thinking that the floating seeds of some plants, rarely rest on water surface; but, over a timescale of several seconds to minutes, these seeds move toward another and, when contained, tend to move toward the exterior walls, such as the breakfast cereals floating in milk often clump together or stick to the walls of the breakfast bowl (*Vella & Mahadeven*; 2005).

The physical explanation of this effect is based on the slope of water surface near the boundaries of the emergent bodies. The Cheerios effect is only the consequence of the forces' presence in proximity of a meniscus drenching the walls.

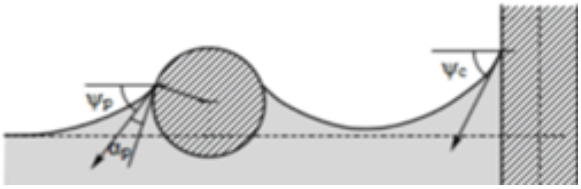

***Fig 1.2**: The menisci studied in this thesis: menisci formed with a particle and cylinder*

1.3 The numerical model

The capture of floating particles, due to a cylindrical collector, can be studied by means of a mathematical model, which is based on the dynamic equations of motion in a two dimensions velocity field and describes the trajectory of a particle that passes close to an emerging cylindrical collector.

1.3.1 The model development

The model is focused on slow flow conditions and small particles. It determines the particle trajectories by integrating the Basset-Boussinesq-Oseen (B.B.O.) (*Umeda & Yang*; 1991).

The B.B.O. equation, modified to deal with floating particles of different geometry, is:

$$\frac{3\pi C_d}{4\sigma L_p}U|U| - \left(\frac{\rho+\alpha}{\rho}\right)\frac{du_p}{dt} + \left(\frac{1+\alpha}{\rho}\right)\frac{du_f}{dt} + \frac{6A_p(\pi v)^{\frac{1}{2}}}{\pi\rho V_p}\int_0^t \frac{(dU/dt')}{(t-t')^{\frac{1}{2}}} = 0 \qquad 2.1$$

here L_p, A_p and V_p are respectively the maximum circumferential length, cross sectional area and volume of a particle immersed in a liquid. C_d is the drag coefficient and ρ is the particle and fluid density ratio: $\rho = \rho_p/\rho_f$. For spherical particles α is a shape

factor given by $\frac{D_p A_p}{3V_p}$ with D_p is the particle draft , as shown in fig. 2.2. $U = u_f - u_p$ is the difference between fluid and particle velocity, while t is the time.

The B.B.O. equation, in its dimensionless form, has been modified considering the capillary forces that are represented by (*Kralchevsky et al.*; 1996):

$$F_c = -\frac{\pi}{2} d_p d_c \sigma \, sin(\alpha_p + \psi_p) \, sin(\psi_p) \, sin(\psi_c) k_1 \, (r/\lambda) \qquad 2.2$$

where r is the distance between the particle and the cylinder, d_p and d_c are the diameters of the particles and cylinders. The others values involved are: ψ_p and ψ_c that represent the curvature angle (for the particle and cylinder respectively) of the meniscus with the horizontal; and α_c that is the contact angle with the cylinder. Finally σ is the value of surface tension (0.073 N/m for water) and k_1 is the modified Bessel function.

The equation 2.1 combined with equation 2.2 gives the equation of the model (*Peruzzo et al.*; 2013) that defines the trajectories (fig. 1.3):

$$\left(\widetilde{\rho_p} + \alpha\right) \frac{d\widetilde{\boldsymbol{u}_p}}{dt} = \frac{3C_D}{4\widetilde{d_p}} \boldsymbol{U}|\boldsymbol{U}| + \\ + \varsigma \frac{6\sqrt{\tilde{\nu}/\pi}}{\widetilde{d_p}} \int_0^t \frac{dU/d\tau}{\sqrt{t-\tau}} d\tau + (1+\alpha) \frac{d\widetilde{\boldsymbol{u}_f}}{dt} - \frac{3}{WeR^2} \sin\left(\theta_p\right) \sin(\psi_c) k_1 \, (r) \hat{\boldsymbol{r}} \qquad 2.3$$

here $R = d_p/d_c$ is the ratio between particle and collector diameter, $\varsigma = A_p d_p / V_p$ and $\alpha = D_p A_p / 3V_p$ are shape factors. For brevity the angle θ_p has been introduced as $\theta_p = \alpha_p + \psi_p$.

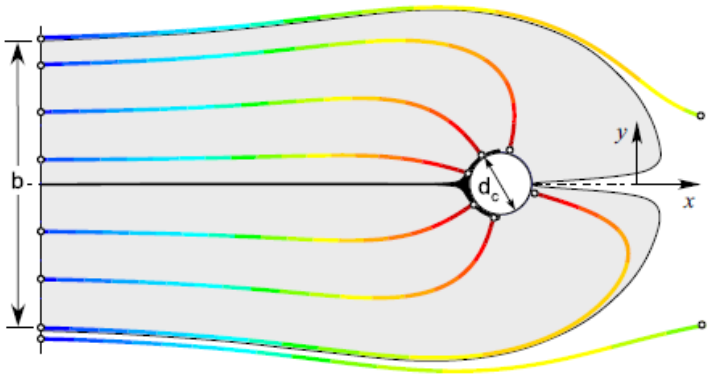

***Fig 1.3**: Trajectories of floating particles, showing the capture area (grey).*

The Weber number (We), that represents the ratio between inertia forces and surface tension, is described by the following formula $We = \rho_f d_c U_0^2/\sigma$ in which U_0 is the velocity of the undisturbed fluid arriving and ρ_f is the water density (1000 kg/m^3 for water).

The drag coefficient C_D is given by *White* (1991):

$$C_D = 24/\left(ReR\left|\tilde{\boldsymbol{U}}\right|\right) + 6/\left(1 + \sqrt{ReR\left|\tilde{\boldsymbol{U}}\right|}\right) + 0.4 \qquad 2.4$$

where the Reynold number Re is the ratio between inertia force and viscous resistance, due to the dynamic process, it is described as $Re = \rho_f d_c U_0/\mu = U_0 d_c/\nu$ in which μ is the dynamic viscosity and ν is the kinetic viscosity.

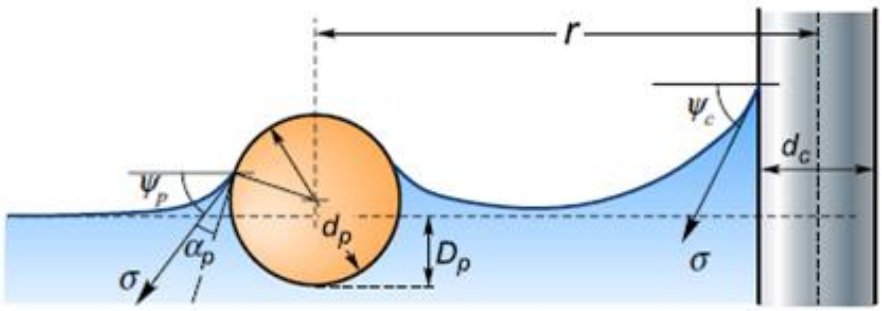

***Fig 1.4**: The values involved in the computation.*

The equation (2.3) illustrates the equilibrium of forces on a buoyant particle: on the right side there are the drag force, Basset history force, added mass force and capillary force.

The solution of the equation is strongly dependent on the values of ψ_p, α_p and Ψ_c. Usually these parameters are computed for hydrophilic sphere with the vertical forces equilibrium.

1.3.2 Evaluation of the meniscus slope

In case of lighter-than-water particle ($\rho_p < \rho_f$), the equilibrium of vertical forces implies that the weight of the sphere and the surface tension are balanced by the pressure force acting on the sphere (*Peruzzo et al.*; 2012) :

$$\frac{\pi d_p^3}{6}\rho_p g + 2\pi r_i \sigma \sin(\psi_p) = \pi h^2 \left(\frac{d_p}{2} - \frac{h}{3}\right)\rho_p g - \rho_p g \Delta h \pi r_i^2 \qquad 2.5$$

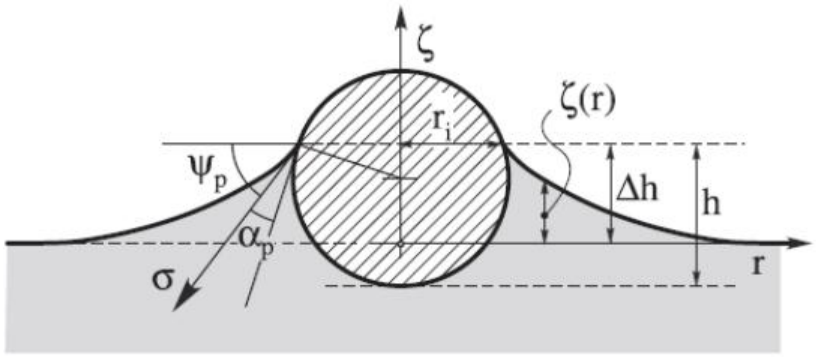

***Fig 1.5**: Angles and specific lengths for a floating light particle ($\rho_p < \rho$).*

From geometrical considerations (fig. 1.5), the contact radius is given by:

$$r_i = d_p \sin\left(\frac{\theta_p}{2}\right) \qquad 2.6$$

By replacing equation 2.6, the equation 2.5 can be rewritten as:

$$\frac{\pi d_p^3}{6}\rho_p g + \pi\sigma \sin(\psi_p)\sin(\theta_p) = \pi h^2 \left(\frac{d_p}{2} - \frac{h}{3}\right)\rho_p g \qquad 2.7$$

The contact radius r_i can also be expressed as:

$$r_i = \sqrt{\left[\frac{d_p^2}{4} - \left(\frac{d_p}{2} - h\right)^2\right]} \qquad 2.8$$

Using the equations 2.6 and 2.8 the sphere immersion h can be expressed as a function of θ_p:

$$h = \frac{d_p}{2}\left[1 + \sqrt{\left(1 - \left(\sin\psi_p\right)^2\right)}\right] = \frac{d_p}{2}\left[1 + \cos\left(\theta_p\right)\right] \qquad 2.9$$

By using the equation 2.9 in 2.7, the equilibrium of the particle is given by:

$$\sin\left(\theta_p\right)\sin\left(\psi_p\right) + Bo\left[\frac{\rho}{6} - \frac{2 + 3\cos\left(\theta_p\right) - \left(\cos\theta_p\right)^3}{24} + \frac{\left(\sin\theta_p\right)^2 \Delta h}{4d_p}\right] = 0 \qquad 2.10$$

where Bo is the Bond number, it represents the ratio between gravitational forces and surface tension and if referred to small particles it can be written as $Bo = \rho_p g d_c^2/\sigma$. It can be observed that for small particles the effects of superficial tension are higher than the gravitational forces. The number can be expressed in this form too: $Bo = \left(d_p/\lambda\right)^2$, λ is the capillary length (equal to almost 2.7 mm for water). $\rho = \rho_p/\rho_f$ is the relative density of the sphere.

The shape of the meniscus wetting the sphere is given by this function:

$$\zeta(r) = r_i \sin\left(\psi_p\right) k_0(r/\lambda) \qquad 2.11$$

where k_0 is the modified Bessel function of order zero.

Replacing equation 2.6 in 2.11 the result is the rise of the meniscus along the contact line of the sphere:

$$\Delta h = \frac{d_p}{2}\sin\left(\theta_p\right)\sin\left(\psi_p\right) k_0\left(\frac{d_p}{2\lambda}\sin\left(\theta_p\right)\right) \qquad 2.12$$

At last, combining equation 2.12 with 2.10 the equilibrium balance becomes (*Peruzzo et al.*; 2012):

$$\sin\left(\theta_p\right)\sin\left(\psi_p\right) + B_0\left[\frac{\rho}{6} - \frac{2 + 3\cos\left(\theta_p\right) - \left(\cos\theta_p\right)^3}{24} + \frac{\left(\sin\theta_p\right)^3 \sin\left(\psi_p\right) k_0\left(\frac{d_p}{2\lambda}\sin\left(\theta_p\right)\right)}{8}\right] = 0 \qquad 2.13$$

Which can be used to compute the meniscus slope angle ψ_p.

2 MATERIALS AND METHODS

In this thesis, three laboratory tests have been performed in order to evaluate the interaction mechanisms between floating particles with two sizes of cylindrical collectors in a uniform water flow.

This chapter describes the experimental apparatus used, with a particular relevance to the flume, cylinders and the particles. The last part deals with the solutions adopted to perform the experiments by varying the flow velocity.

2.1 The Flume

The experimental apparatus used consists of a 4 m long flume located in the Hydraulic Laboratory of the ICEA Department. It is characterized by a rectangular section of width 75 cm and height 20 cm; the walls and the bottom are made of transparent plexiglas (fig. 2.1).

The channel can be tilted with a threaded screw fixed to a support (fig. 2.2a). The slope is for this reason measured by a pointer (fig. 2.2b).

***Fig 2.1**: The flume used*

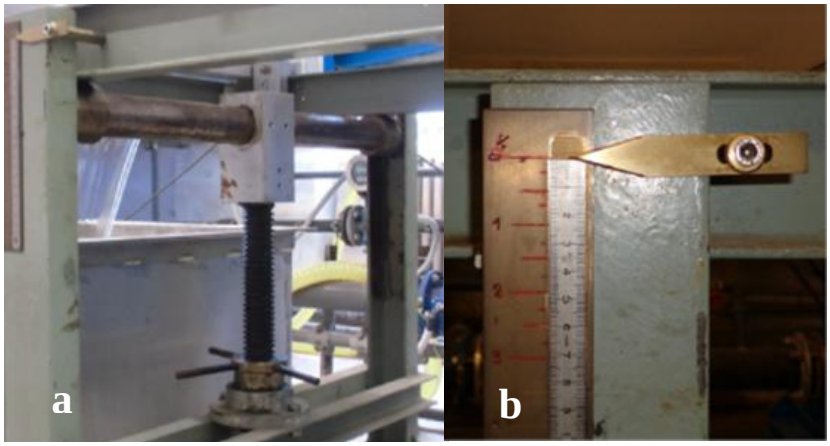

***Fig 2.2**: The flume's accessories during an experimental investigation. (a) The threated screw and (b) the slope indicator.*

In these three experiments the slope is fixed at the value of $i = 0.0$, i.e. the bottom was flat during the experiments. The outflow is regulated with a gate (fig. 2.2b).

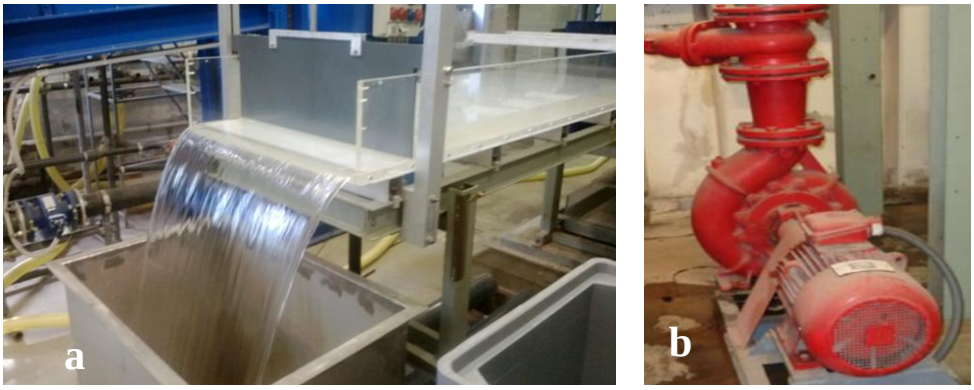

***Fig 2.3**: The flume's components. (a) The gate and (b) the centrifugal pump.*

Downstream of the gate a tank collects the outflow (fig. 2.3a) and by two drains the water is stored in a bigger tank placed under the flume. A centrifugal pump (fig. 2.3b) raises the water from the storage tank up to the head tank (fig. 2.4a). The channel is fed by a conduit equipped with a magnetic flow meter (fig. 2.4b). This instrument lets us know the flow of the flume, and, in case, it can be modified with a crank (fig. 2.4c) up to the maximum value of 30 l/s.

***Fig 2.4**: The flow regulation. (a) The head tank, (b) the flow meter and (c) the crank.*

The flow in the inlet is far for being uniformly distributed, and for this reason a wall of bricks has been assembled in the upstream section of the flume (fig. 2.5a).

After having fixed the water flow and the opening of the gate, a time of about 5 minutes has been needed to stabilize the flow conditions.

In order to record the particle patterns, on the wall along the right side of the flume was fixed a support where the camera has been placed in the longitudinal axis of the channel (fig. 2.5b).

***Fig 2.5**: Flume's accessories to carry on the tests: (a) wall of brick, (b) camera's support.*

2.2 The Cylinders

In the experimental investigations two maple cylinders of size d= 3 mm (named cylinder 1) and d= 6 mm (labeled as cylinder 2) have been used.

One cylinder per time was fixed into a base and upright perpendicular to the flow (fig. 2.6a). In each series cylinder 1 and cylinder 2 have been posed between the lateral walls in the average position for all the test duration.

A digital camera has been set exactly over the cylinders (fig. 2.6b) and it allows the videos extraction to study the flow velocity and the trajectories of the particles.

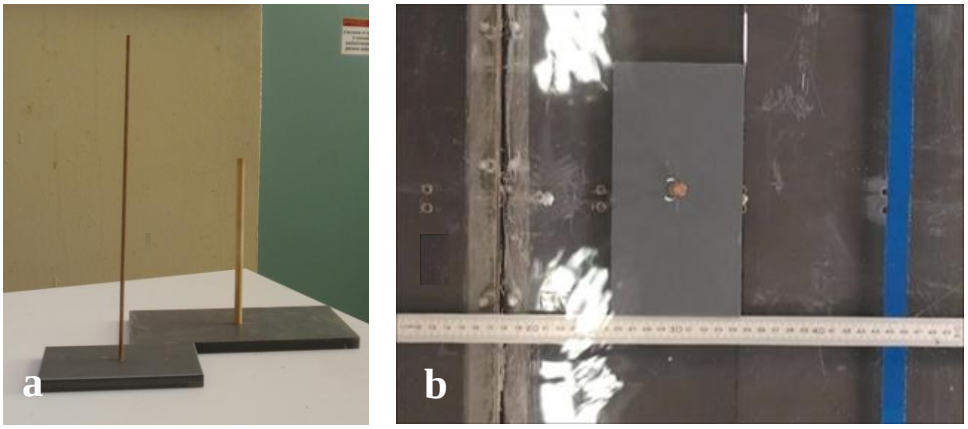

***Fig 2.6**: The cylinders. (a) Frontal vision of cylinders, (b) a result of camera positioning over a 0.6 cm diameter cylinder.*

2.3 The particles

To simulate the plant seeds, four size of EPS particles (with an approximately spherical shape) have been chosen; the diameters of the particles are: $2 < d_p < 6$ mm (fig. 2.7). The choice of EPS particle was given by its small density (ρ_p = 35 kg/m^3); as well known lighter particle are more susceptible of capillary attraction and thus it is more easy study the Cheerios effect in our experiments.

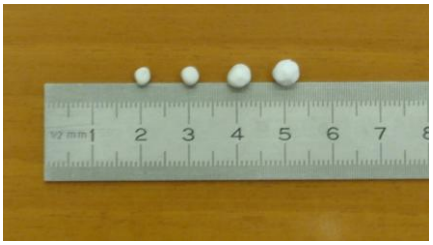

***Fig 2.7**: The used particles.*

The particles are characterized by a nominal diameter (Tab 2.1), that has been taken into account during experimental investigations, and by a measured diameter (that represents the actual dimension of a particle). The measured diameter was estimated by frame analysis of sample of particle that have been assumed having the same size. Through a comparison between size of the particle and a meter graduated in the picture we was able to extract a statistic of the particle sample used in the experiments.

***Tab 2.1**: the table contains the nominal diameter used as reference during the tests and the actual values of the particle (mean value measured and standard deviation).*

Nominal Diameter (mm)	*Measured Diameter (mm)*
2	2.64±0.39
3	3.88±0.36
4	4.43±0.77
5	5.76±0.84

2.4 Description of the laboratory methodology

The procedure followed during the experimental investigations is the same for the three cases this thesis deals with; however before explaining it, it is necessary to portray the condition to obtain effective results: having a uniform (or nearly uniform) flow velocity.

2.4.1 Creation of uniform flow and velocities computation

In this thesis, for every case of uniform flow, it has been considered a specific water velocity and opening of the gate (the bottom slope, as said before, was fixed equal 0 for all tests). To obtain this state of flow two length of 45 cm (fig. 2.8a) and 70 cm (fig. 2.8b) have been highlighted by using scotch tape fixed at the bottom. After having imposed the flow and the opening of the gate, it was necessary to wait some minutes in order to stabilize the water circulation. A spherical particle with a nominal diameter of

6 mm has been released before the first colored line and the time spent to cover the first distance of 45 cm was measured by a chronometer. The travel times of the particle has been measured for more than ten runs in order to obtain a statistic. The same steps have been done by measuring the time for the second distance of 70 cm. The comparison of the two mean velocity measured allows to ascertain the uniform (or near to be uniform) flow condition in that part of the flume. If values were different the gate and/or the water flow were adjusted and new particle runs were measured until uniform flow condition has been reached.

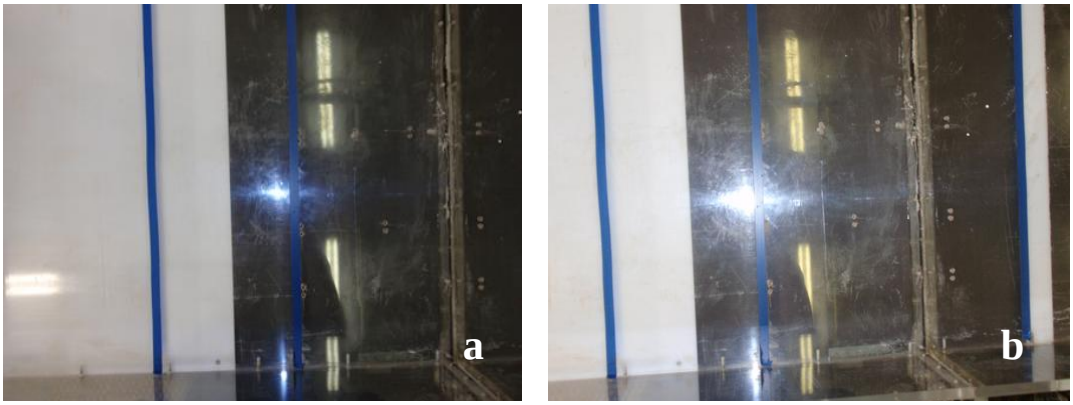

***Fig 2.8**: The involved lengths. (a) 45 cm and (b) 70 cm.*

For every series the standard deviations was also computed to assure that the difference of velocity in time can be considered negligible. The velocity, assumed as laboratory result, is the mean between the velocities in the two lengths. For the experiments three flow velocities were assumed. In Tab. 2.2 are summarized all flume conditions for the cases analyzed, and fig. 2.9 shows the velocity measured for every runs in all three cases.

***Tab 2.2** : The table synthesizes the values of the water flow, Re, slope of the channel and the opening of the gate for every case; it considers both the length of 45 cm and 70 cm.*

	Re		**Gate opening (mm)**	**Q (l/s)**	v_{45}**(cm/s)**	σ_{45}*(cm/s)*	v_{70}**(cm/s)**	σ_{70}*(cm/s)*
	d_c=3mm	**d_c=6mm**						
Case 1	290	577	5	2.7-3	9.6	0.04	9.6	0.04
Case 2	217	433	3	2.6-2.8	7.2	0.037	7.2	0.02
Case 3	391	782	7	3.4-3.5	13	0.09	13	0.05

	L_1= 45 cm	L_2= 70 cm	$\overrightarrow{v_{lab}}$ (cm/s)
Case 1	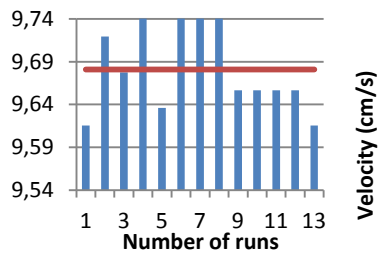	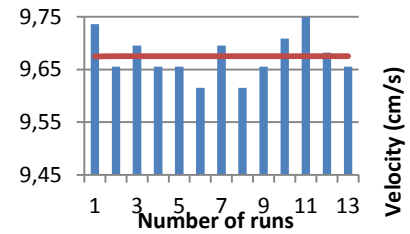	9.6
Case 2	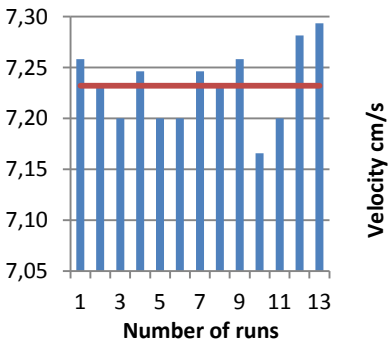	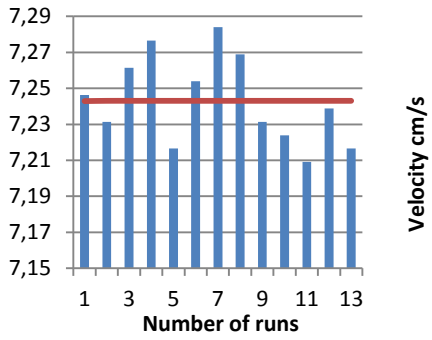	7.2
Case 3	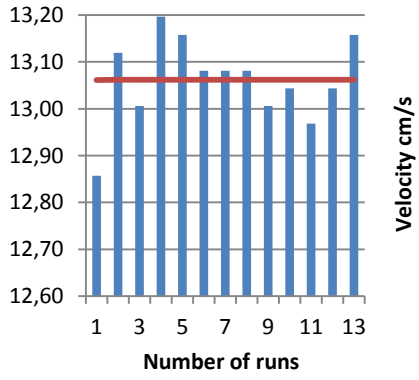	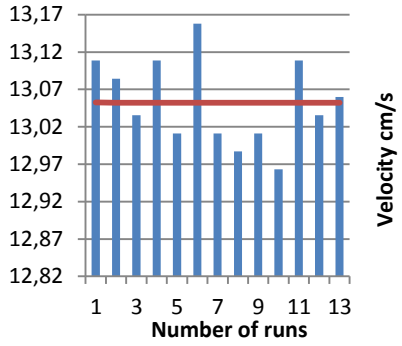	13

***Fig 2.9**: The table represents the three cases; for every one of them both the length of 45 cm and 70 cm are represented. The graphs in the x axis labels the runs (always thirteen) and in the y axis their velocities. The red line is the mean velocity. The last column indicates the laboratory velocities assumed.*

In order to have a further check of the obtained results, the undisturbed particle velocities have been estimated also by the video analysis both as instantaneous velocity and mean velocity. The instantaneous velocity was estimated by the ratio between the distance travel by the particle and the time between two frames in sequence, i.e. 0.04 s being the acquisition rate of the camera equal to 25 Hz . This analysis is more accurate and represents the actual velocity in the experiments.

For estimating the mean velocities, for every path, were considered two lengths: *i)* the first ten frames recorded and *ii)* the next ten frames, in order to observe small difference in terms of velocity and standard deviation.

***Tab 2.3**: the table for every case reports the velocities pre and post processed (mean velocity and the mean of instantaneous velocities); the third and fifth columns label the standard deviations between laboratory and calculated values.*

	v_c (cm/s)	σ_c(cm/s)
Case 1	7.8	0.47
Case 2	6.2	0.7
Case 3	11.8	0.8

In Tab. 2.3 are summarized the velocities measured in the three cases of analysis with the difference methods explained, i.e. preliminary velocity measured and the mean velocity by video analysis. The result of this analysis is given by the standard deviations that, being represented by low values, indicate a good agreement between laboratory and computational results.

2.4.2 The experiments

In the experiments, all the cases are composed by two series of tests, *i)* with the cylinder of 3 mm of diameter and *ii)* with the cylinder of 6 mm. In all experiments 25 cm upstream of the cylinder the particle have been released and its path recorded by the camera. Between the recorded path only fifteen runs for each series are available, i.e. the particle paths in which trapping or a strong particle deviation occur.

Three of these videos, generally the ones with peculiarities in their motion, have been chosen to reconstruct the trajectories as described in the Chapter 3.

A fourth video, that near to have a straight flow, has been used to fix the size of the particles. At the bottom of the flume a ruler was posed to compute the scale factor

2.4.3 Description of the statistical analysis to assign the size of the particle

The Autocad Map diameters are known after having centered the particles, for this reason, the problem was to assign the actual values of them. The followed procedure is described in the next part.

After having chosen a video and obtained the frames (using the program JPG converter), the research considers fifteen consecutive images as upstream as possible from the cylinder.

Every frame has been inserted in *Autocad Map* and, centering the sphere, a diameter for every image has been given. In this way, very similar values have been obtained; after having computed the statistics (mean and variance) of the diameters, the mean value has been assigned to the particle.

After having defined the scale factor (*FS*) as the ratio between the unit length in the free surface and at the bottom, a control has been developed: because of the water level is not so high, the scale factor should show almost an equal length, therefore values in the interval 0.8-0.98.

For this reason the research verifies that the *Autocad Map* diameters allow this range. It must be pointed out that in some trajectories the images composing a path had a slightly different size from the standard values proposed in Tab. 2.1. In the Tab. 2.4 the values obtained and used are reported:

***Tab 2.4**: values of the particles' diameters both with 6 mm cylinder and 3mm.*

Case 1 (v = 9.6 cm/s)	**$d_{particle}$ (cm) – Cylinder 0.3cm**	**$d_{particle}$ (cm) – Cylinder 0.6cm**
A	0.262	0.299
B	0.353	0.355
C	0.42	0.465
D	0.564	0.595
Case 2 (v = 7.2 cm/s)	**$d_{particle}$ (cm) – Cylinder 0.3cm**	**$d_{particle}$ (cm) – Cylinder 0.6cm**
A	0.248	0.23
B	0.322	0.278
C	0.375	0.414
D	0.545	0.505
Case 3 (v = 13 cm/s)	**$d_{particle}$ (cm) – Cylinder 0.3cm**	**$d_{particle}$ (cm) – Cylinder 0.6cm**
A	0.225	0.25
B	0.352	0.304
C	0.37	0.358
D	0.592	0.492

3 ANALYSES OF THE TRAJECTORIES

The first part of this chapter deals with the criteria that has been adopted to reconstruct the particles' paths, starting from the frames captured during the experiments, as described in the previous part. In the second part it is described the procedure to estimate the trajectories through the physically-based model and, finally the comparison between numerical and experimental results.

3.1 Trajectories from available data

The main available data for each cylinder are the video in which are recorded the paths of all the used particles. The runs with strong interaction or trapping have been cut from the recorded video of the experiments by using the program *Movie Maker*. Totally are available fifteen successful runs for every particle.

Once these videos have been selected, all their frames were extracted through the program *JPG converter*.

Subsequently, for a fixed collector and particle, the obtained images have been imported in the environment of *Autocad Map* (fig. 3.1).

The cylinder of the first inserted frame, has been highlighted in red colour and it has been assumed as the centre of the analysis domain (fig. 3.2), i.e. a square of length equal to side 20 d_c (fig 3.3). Each frame, whose particle appears inside of the domain (fig. 3.4), has been inserted and the sphere has been marked with a colour (different for every particle's diameter) (fig. 3.5).

Particle paths belonging at the same case of analysis were then pasted in the same domain centred in the origin of *x-y* axes (fig. 3.6a-b), in order to summarize the existing information on the case of study.

Finally, to compare the numerical and experimental paths, each domain is scaled in non-dimensional square of size 20x20, i.e. the cylinder is considered the scale length of the problem (fig. 3.7a-b) .

The procedure has been repeated for every case, totally twenty-four paths are available (eight for every case: four with the 3 mm cylinder and four with 6 mm cylinder).

Please note that some errors can affect the position of the particle in the domain, as parallax effect, wrong alignment of the camera and user-error due to the not clear image of the particle when it moves with quite high velocity. Although the procedure adopted is quite rough, the accuracy of the position can be assumed with a total error of 0.1 d_p.

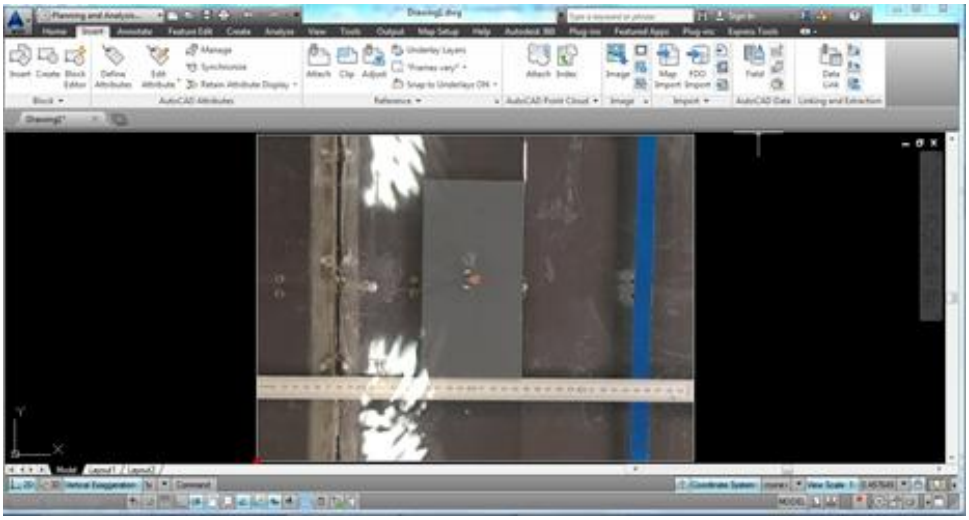

***Fig 3.1**: Example of image importation in Autocad Map.*

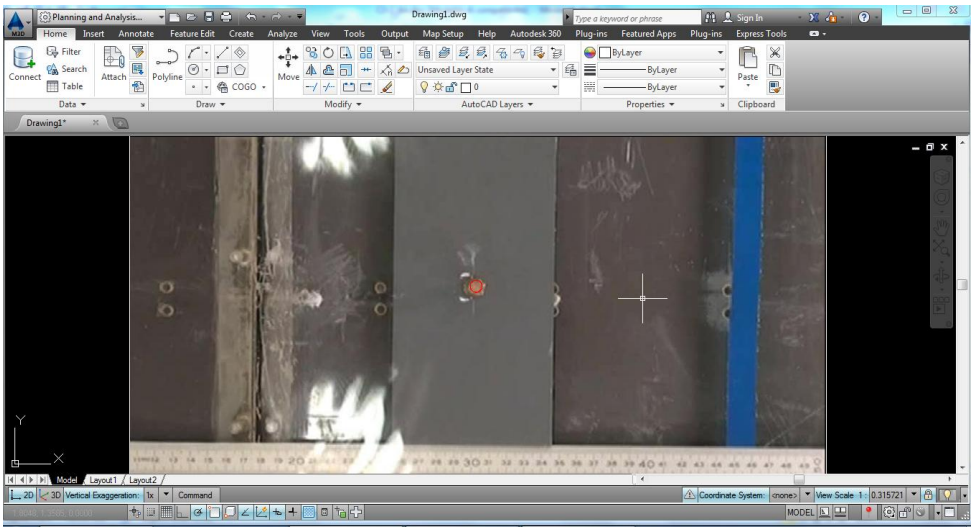

***Fig 3.2**: The cylinder has been centered in red colour.*

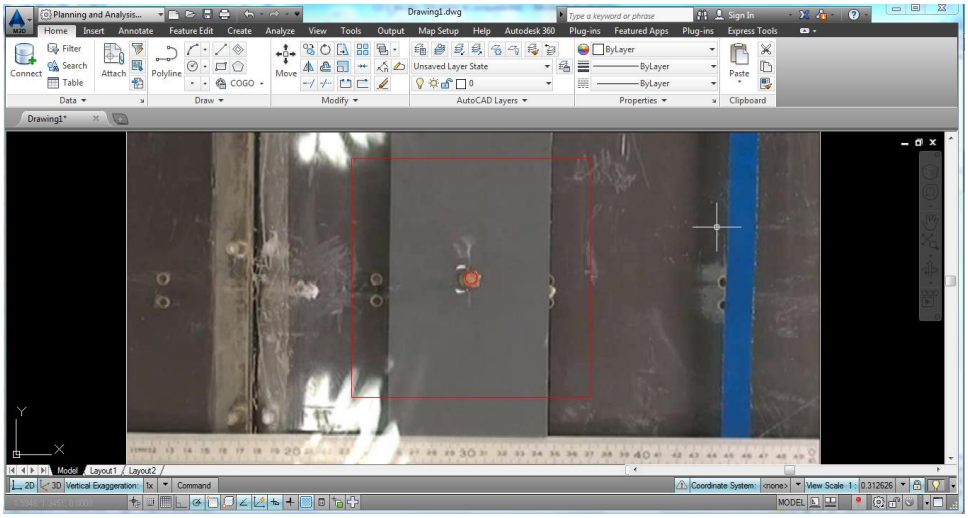

***Fig 3.3**: A square of side 20 d_c has been created.*

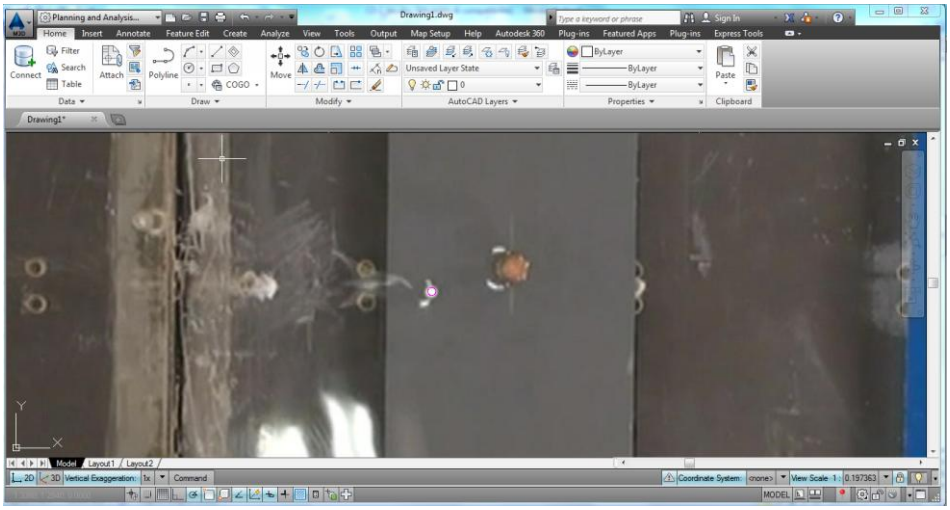

***Fig 3.4**: The particle has been signed in another image.*

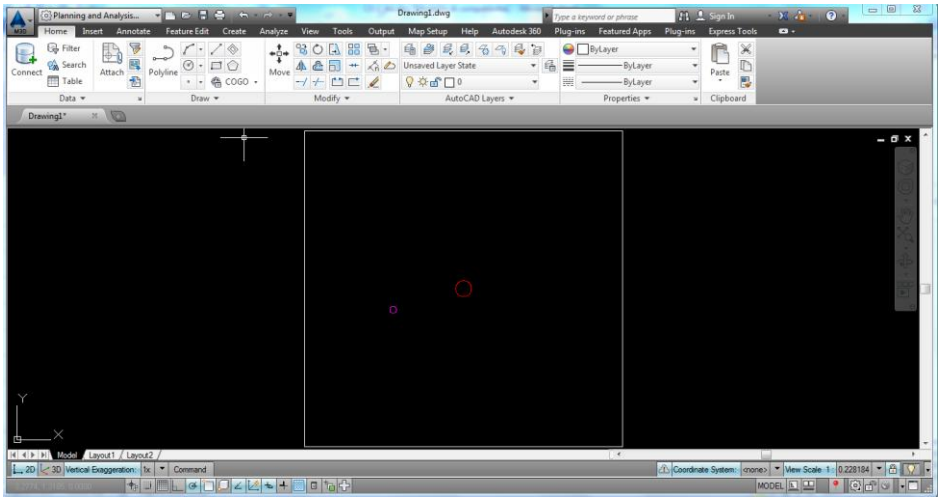

***Fig 3.5**: The image removal.*

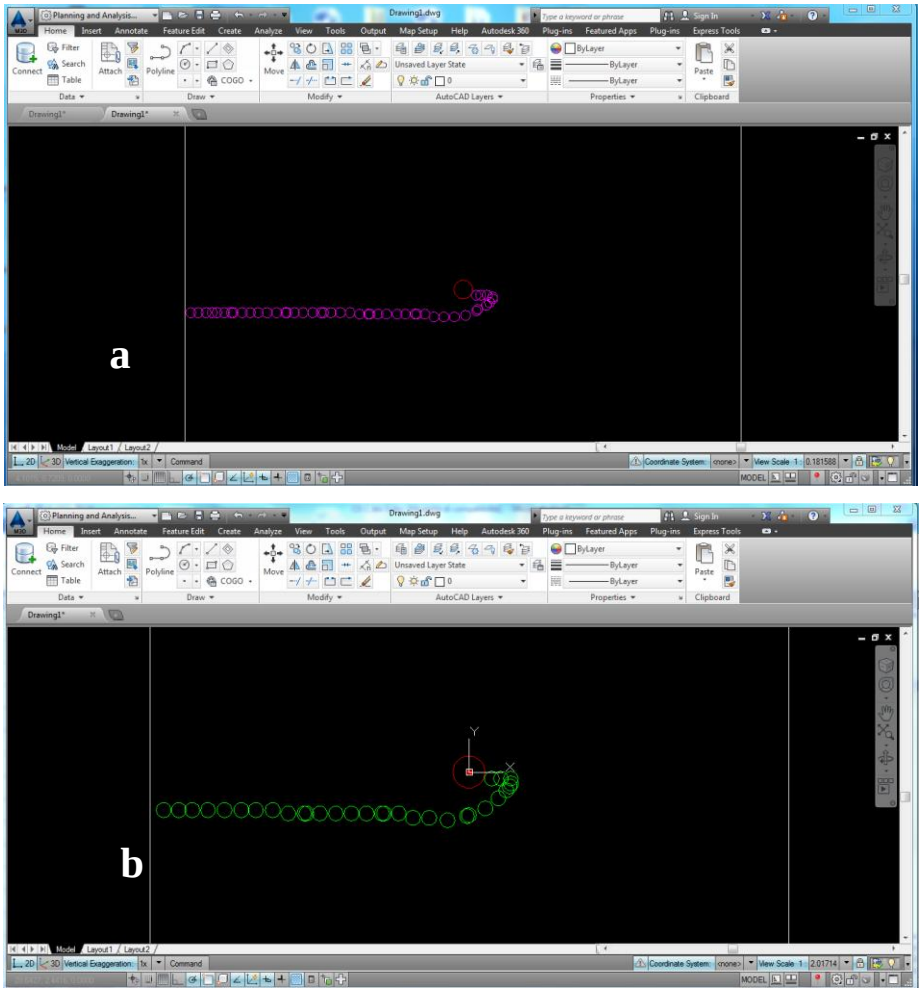

***Fig 3.6**: The path reconstruction. (a) the x-y origin is in AutocadMap environment, (b) the x-y origin has been moved in the cylinder center.*

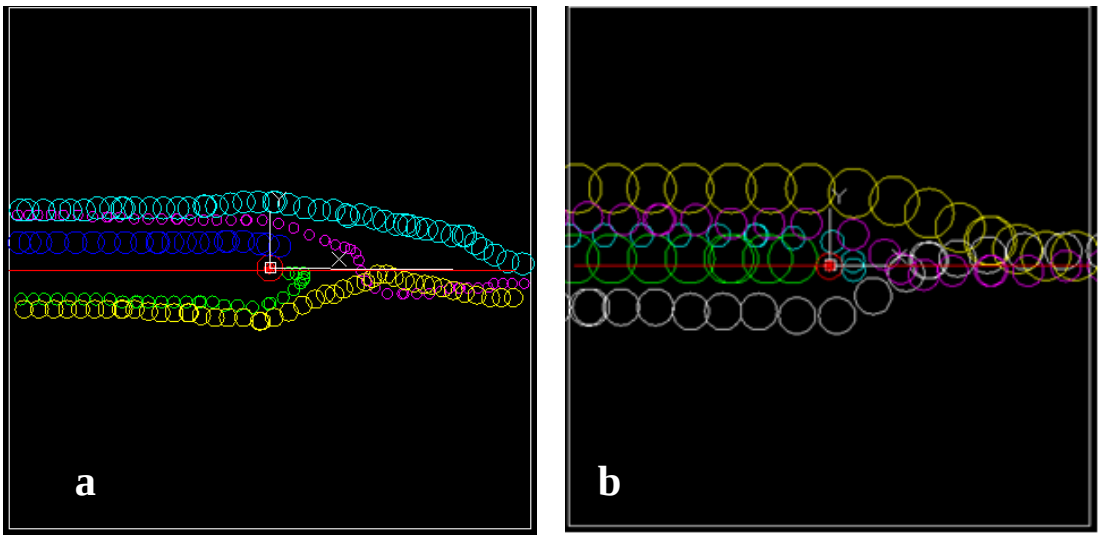

***Fig 3.7**: Examples of the trajectories obtained. (a) Case two, Cylinder's diameters 6mm; (b) Case 1, Cylinder's diameter 3mm.*

3.2 Trajectories computed by the numerical model

As described in the Chapter 1 (paragraph 1.3) the path of small floating particle flowing close to a single emergent cylinder can be simulated by integrating the dynamic eq. (2.3) by a semi-implicit scheme.

Peruzzo et al. (2013) proposed a physically-based model to reconstruct particle trajectories starting from the geometry (e.g. size of particle d_p and diameter of the collector d_c) and hydrodynamic condition (e.g. fluid velocity U_0) of the problem, with the assumption of small Reynolds number, i.e. $Re < 48$ ($Re = d_c U_0/\upsilon$), so that no vortex shedding onset occurs.

The numerical model has as input file the non-dimensional velocity field that is extracted with a regular grid from the domain of analysis (a square of size 20x20 centered in the collector, i.e. the same domain adopted in the experimental analysis) (fig. 3.8). The velocities are computed by a *FEM* commercial software (*Comsol Multiphysics*) in which the cylinder diameter and the undisturbed flow velocity are fixed to $d_c = 1$ and $u_0 = 1$ respectively. The velocity field is evaluated for different Reynolds

number *Re* by varying the kinematic viscosity ν, that in this non-dimensional study assumes fictitious values.

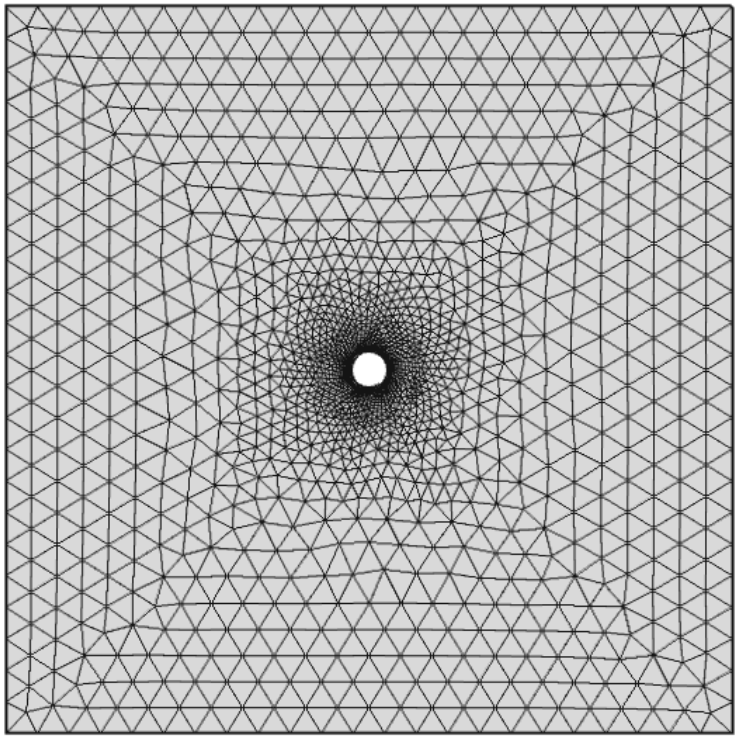

Fig.3.8: *Mesh of the domain of analysis. The collector (size d_c) is placed in the center of the square with length of 20 d_c.*

To compare the numerical and experimental particle trajectories, the numerical model has to be modified to take into account the unsteady flow condition on the backside of the collector, due to the vortex shedding onset. Indeed the Reynolds number of the experiments ranges between 200 and 700, i.e. the typical range in which vortex shedding is observed in several wetland areas.

In this case a single velocity field cannot fully describe the phenomenon, thus, once the vortex shedding has reached the equilibrium in *Comsol* simulations, several velocities fields are exported with a fixed time step of $\Delta t = 0.2\ d_c/U_0$ during a single period of vortex shedding *T*. It is worth noting that the simulated period *T* is in according to the observed period of vortex shedding evaluated by experimental data by *Fey et al.* (1998). The results of which have been explained in the Section 1.3. Fig 3.9 shows an example of vortex shedding simulated by the software.

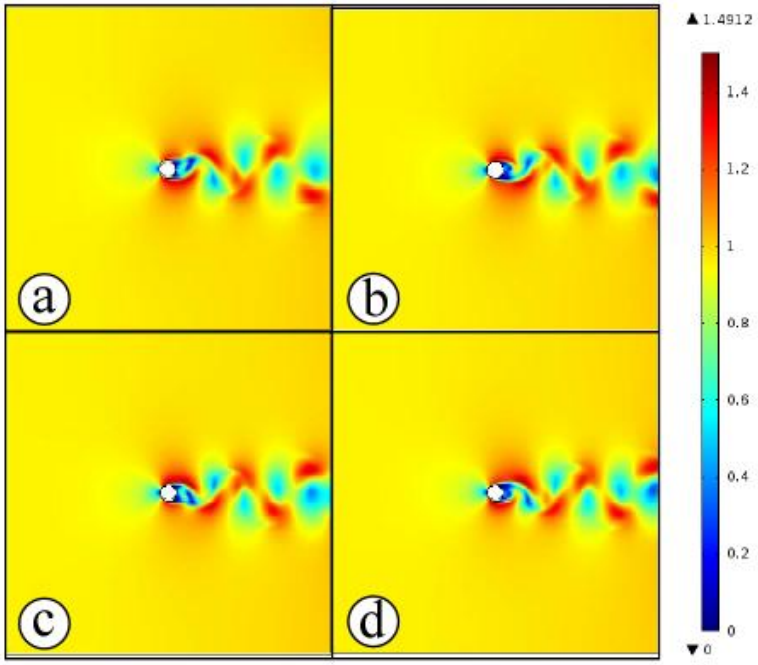

***Fig 3.9**: Velocity field simulated by Comsol for Re=220 (a) t= 0, (b) t= T/4, (c) t=T/2 and (d) t= 3 T/4.*

When the path is integrated with time *t* the flow velocity in the particle position is estimated by linearizing the velocity both in space and in time between two recorded velocity fields; in case of which the duration of the particle travel exceeds the period *T*, the model reloads the hydrodynamic in loop mode.

The particle run needs to set up the model parameters into the input file named *parametri.txt* (fig. 3.9). Specifically a first set of parameters defines the computational options, such as the method of input of the parameter (manually or by the physics of the problem), the tolerance *toll* below of which the solution is accepted, the time step of integration *dt* and the interval of time between two printed solution Δt_{print}.

In a second set are reported the values of the parameters introduced in the eq. (2.3) in non-dimensional form: the type of particle (label *0* indicates sphere shape), the initial position of the particle x_{p0} and y_{p0}, the ratio between particle and cylinder size *R*, the Reynolds number *Re*, the Weber number *We*, the relative density of the particle with the fluid density ρ_r, the ratio between cylinder size and capillary length $\lambda^* = d_c/\lambda$, the Bond number *Bo*, the contact angle of particle α_p, the particle meniscus slope ψ_p

(evaluated by eq. (2.13)) and the collector meniscus slope ψ_c. Note that if the value of ψ_p is negative, the model computes automatically the meniscus slope by solving the floating equation of a small hydrophilic particle (eq. 2.13).

The last two parameters are introduced to load the hydrodynamics in vortex shedding condition, i.e. the vortex shedding period T (expressed in this analysis with the unit scale d_c/u_0) and the period of time between two exported solution Δt_T.

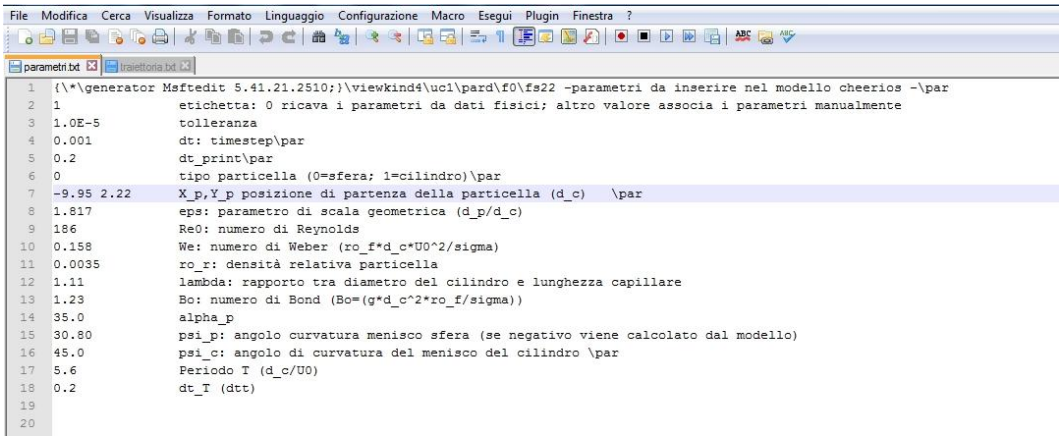

***Fig 3.10**: An example of the input file parametri.txt.*

The model compute the path of the particle until it collides the collector or exits the domain. The output file *traiettoria.txt* shows in five columns the time t, the position of the particle into the domain x_p and y_p and the longitudinal and transversal velocity u_p and v_p.

Finally the output file has been transferred in Excel to create a polyline to load in AutoCAD Map in the same domain of experimental trajectories..

The comparison between experimental and numerical paths has been done initially by adopting the same initial particle position, x_{p0} and y_{p0}, in the inlet section of the domain. A sensitive analysis were performed in order to evaluated the accuracy of the computed solution, and sometimes the numerical path has been corrected by adjusting the position of the particle y_{p0}. In Tab. 3.1-3 are summarized the parameters of the input file used to draw the trajectories in the three cases of study

Tab 3.1: Table of the value used in the model for the case one

Case 1										
d_p *(mm)*	d_c *(mm)*	*R*	d_c/λ	*Bo*	v_c*(cm/s)*	*Re*	*We*	α_p *(°)*	y_p *(°)*	y_{p0}
2.62	3	0.87	1.36	1.85	7.8	234	0.25	35	10.96	-1.19
3.53		1.17							17.02	1.78
4.2		1.4							21.66	-1.69
5.64		1.88							31.1	2.99
3	6	0.5	2.72	7.4		468	0.5		13.45	-1
3.55		0.6							17.16	1.69

Tab 3.2: Table of the value used in the model for the case two

Case 2										
d_p *(mm)*	d_c *(mm)*	*R*	d_c/λ	*Bo*	v_c*(cm/s)*	*Re*	*We*	α_p *(°)*	y_p *(°)*	y_{p0}
2.48	3	0.82	1.36	1.85	6.2	182	0.158	35	10.06	-1.83
3.22		1.07							14.92	-2.27
3.75		1.25							18.53	2.44
5.45		1.81							30.8	2.22
2.3	6	0.38	2.72	7.4		372	0.316		8.93	1.9
2.78		0.46							12	-1.12
4.14		0.69							21.24	-1.58
5.05		0.84							27.7	2.23

Tab 3.2: Table of the value used in the model for the case three

Case 3										
d_p *(mm)*	d_c *(mm)*	*R*	d_c/λ	*Bo*	v_c*(cm/s)*	*Re*	*We*	α_p *(°)*	y_p *(°)*	y_{p0}
3.04	6	0.5	1.38	1.9	11.8	708	1.144	35	13.71	-0.46

3.3 Results and discussion

The paths obtained with the numerical model and the laboratory data, are here represented, for the most significant cases, respectively with successions of particles and a continuous lines; these results allow us to argue on the trapping mechanisms. The comparison is done only by qualitative analysis because the formulation of quantitative parameters that can synthetize the likelihood of the solutions is hardly feasible.

Most of the trajectories obtained from the numerical data are very similar to the graphical representation given by the model, and in both cases in proximity of the cylinder, the spheres tend to be more spaced, i.e. the velocity is increasing because of the Cheerios effect. It means that the effect of capillary force, such as the deviation or trapping can be predicted with a good approximation in some cases (fig. 3.11).

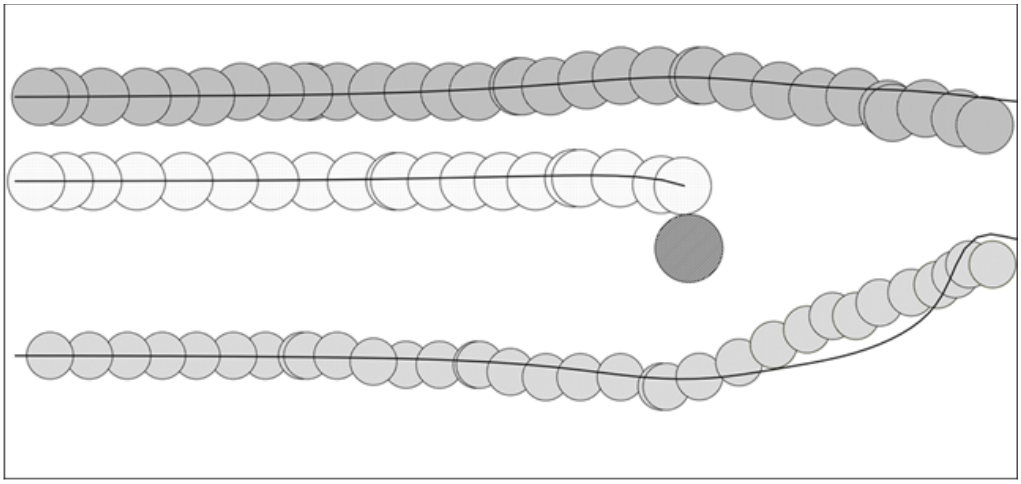

Fig 3.11*: Representation of the model (lines) and observed (succession of particles) trajectories. The figure regards the case 2 (U_0= 7.2cm/s) with a cylinder's diameter equal to 6 mm. The higher paths (in AutocadMap: blue and Cyan) have a diameter of 5 mm while the other (yellow) of 4 mm*

It can be observed that the number of particles' trapping is lower than their deviations from the original path, in particular some of them get stuck with the cylinder in its frontal portion that is directly exposed to the flow (these images are omitted because doesn't give important information). As observed in previous experiments several trapped particle move toward on the backside of the collector from the original

place where they encounter the cylinder (fig. 3.12). For low velocity, i.e. low *Re*, particle can be trapped directly on the backside of the collector (fig. 3.13); this result is also predicted in the study of *Peruzzo et al.* (2013) (fig 1.3 in Section 1.3.1) and it reinforces the robustness of the proposed solution. However the path shown in fig. 3.13 is found by shifting the initial position of the particle of 0.15 d_p, i.e. 0.5 mm, and this lets some considerations: *i)* small error in the position of the particle for the most external capture can produce opposite results, i.e. capture or not capture of the particle, *ii)* the particle path in case of capture on the backside part might be unstable, i.e. it is strongly affected by small variation in the hydrodynamic condition, and *iii)* the numerical trajectories moves toward the collector less than in the experimental one, because the capillary force is underestimated for small distance between particle and cylinder.

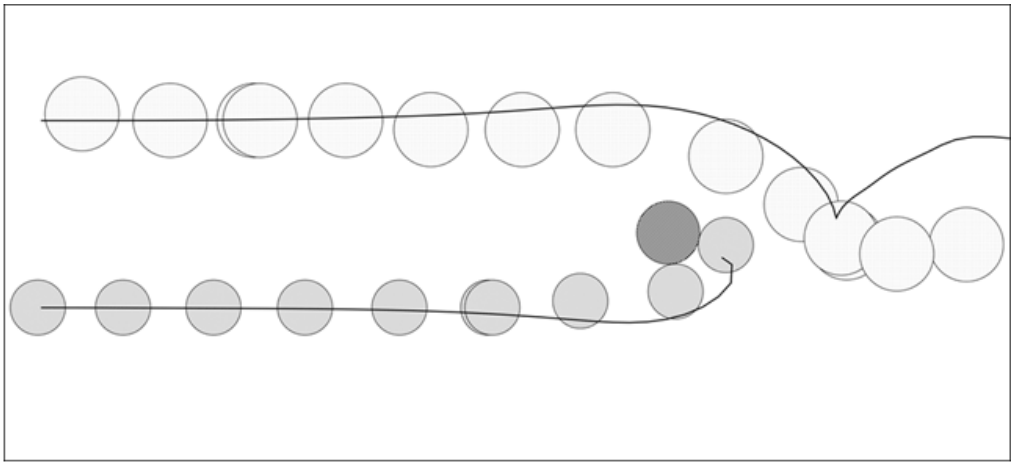

***Fig 3.12**: An example of a flow (with vortices downstream of the cylinder) where the model satisfactorily represents the trajectories of the smaller particles. The figure regards the case 1 with the cylinder's diameter of 3 mm. The trapped particle (in AutocadMap blue) has a diameter of 2.5 mm while the other (in AutocadMap Magenta) a diameter of 3.5 mm*

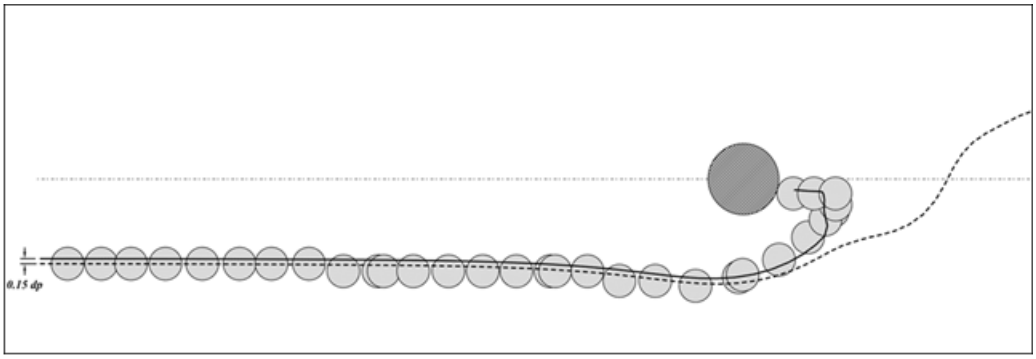

***Fig 3.13**: It describes the trajectory observed (succession of particles) and the numerical results (dashed line). The continuous line represents the numerical solution after having shifted of 0.5 mm the initial particle. The image regards case 2 (U_0=7.2 cm/s) and the 6 mm cylinder. The particle diameter is of 2.8 mm and in AutocadMap is represented in green*

Another path collected during the experiments (fig. 3.14) may confirm the actual underestimation of the capillary force in the model: the numerical trajectory overlaps very well all the experimental data, but the particle is not captured as observed in laboratory because the force acted on the actual particle has greater magnitude just when the distance is very small.

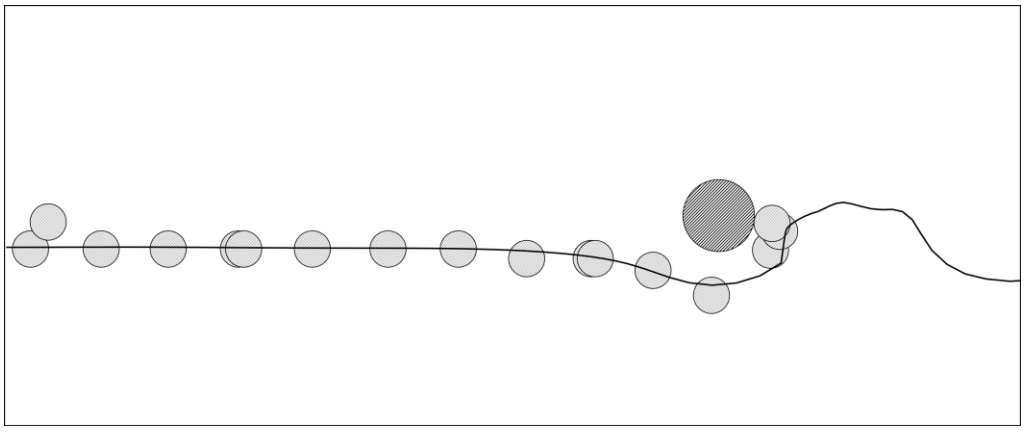

***Fig 3.14**: An example of results that underlines the understimation of the capillary forces. The result regards the case 3 (U_0=13 cm/s) and the 6mm cylinder. The path of the 3.2 mm particle in AutocadMap is represented in blue.*

This difference is a consequence of the linearized solution adopted for the Laplace problem of the capillarity, solution that is expressed by the eq. 2.2. It well known that the force F_c is well estimated only for small particle and cylinder (d_p, $d_c < \lambda$) and for large distance L between the two bodies ($L >> \lambda$) (*Kralchevsky & Denkov;* 2001), but experimental evidences of the error due to this approximation lacked.

What said above is also verified by the comparison of the trajectories in fig. 3.15a and in fig. 3.15b in which gap between numerical and experimental results appear when the particle is near to the collector; this gap increases when particle size increases (compare the particle paths of fig. 3.11, in which the transversal distance between the particle is the same) and when the particle is closer to the collector, e.g. trajectories comparison between the larger and farthest particle with the smaller and closer one.

A more detailed analysis highlights small differences in representing particles' trapping or deviation with the model or with the laboratory procedure.

The particles that are not captured, once passed the cylinder, can significantly change their directions because of the presence of alternated vortices.

In most cases, the two solutions find a good overlap upstream of the cylinder while downstream the actual result is slightly different from the calculated one (fig. 3.7a). The causes of this imprecision may be that *i)* in the model the particle experienced a flow velocity that is assumed being the velocity on the centroid, thus it may not represent the actual distribution of the velocity on the entire particle *ii)* the numerical and experimental particle experienced different phase of vortex shedding when the particle past the cylinder fig. 3.16 shows an example of sensitivity analysis, in which the phase of numerical vortex shedding was shifted of *T/2*. In the vortex shedding area two different paths are observed, but the difference is small to match the actual particle trajectory.

The cause *i)* is supported from the result reported in fig. 3.17. The path followed by grey particle shows how the numerical solution can be susceptible to heterogeneous velocity field and this behaviour it is not observed in the experimental solution.

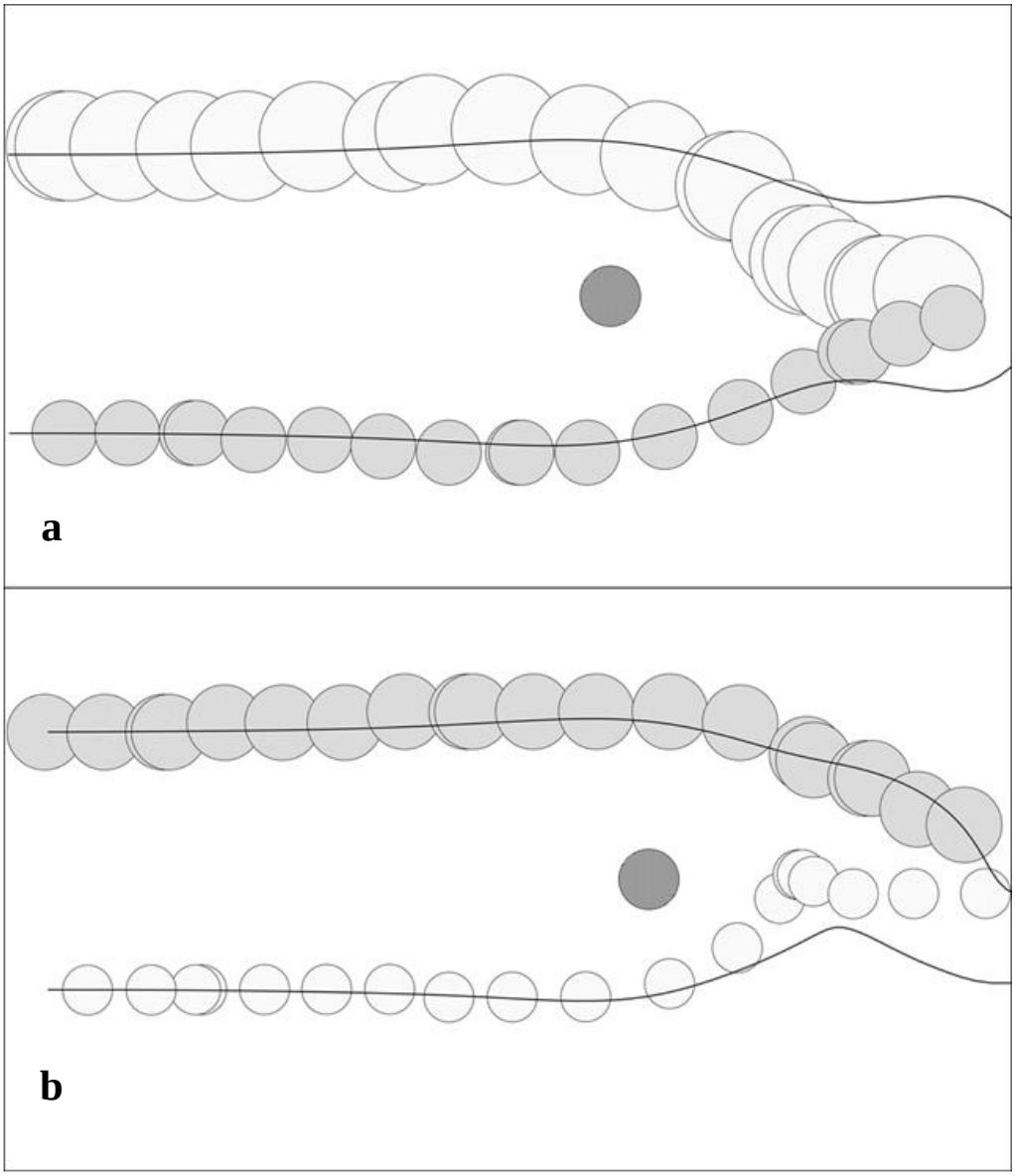

Fig 3.15*: The results of the case 1 with cylinder's diameter of 6 mm, it is the flow with the lower velocity. (a) a good agreement between actual and computed pat;h the higher particle (yellow in AutocadMap) has a 5 mm diameter and the lower (white) of 3 mm.; (b) another case of good result but for the lighter particle only upstream of the cylinder. The first particle (green) has a diameter of 4 mm and the second (blue) of 2.5 mm*

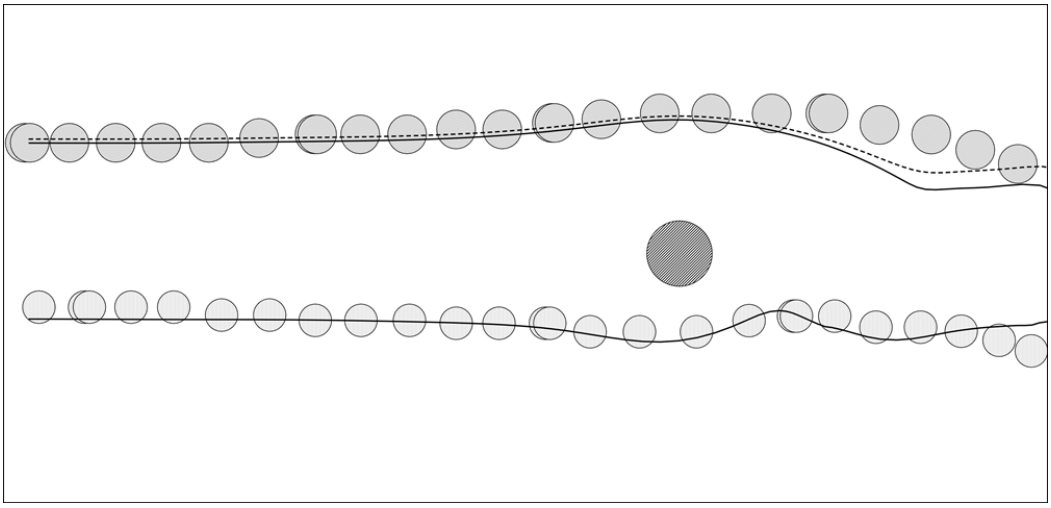

***Fig 3.16**: The numerical and observed results for the case 1 with a cylinder's diameter of 0.6 mm. The upper particle (magenta in AutocadMap) has a diameter of 3.5 mm while the lower (yellow in AutocadMap) of 0.3 mm. The result is an example of different phase in the paths.*

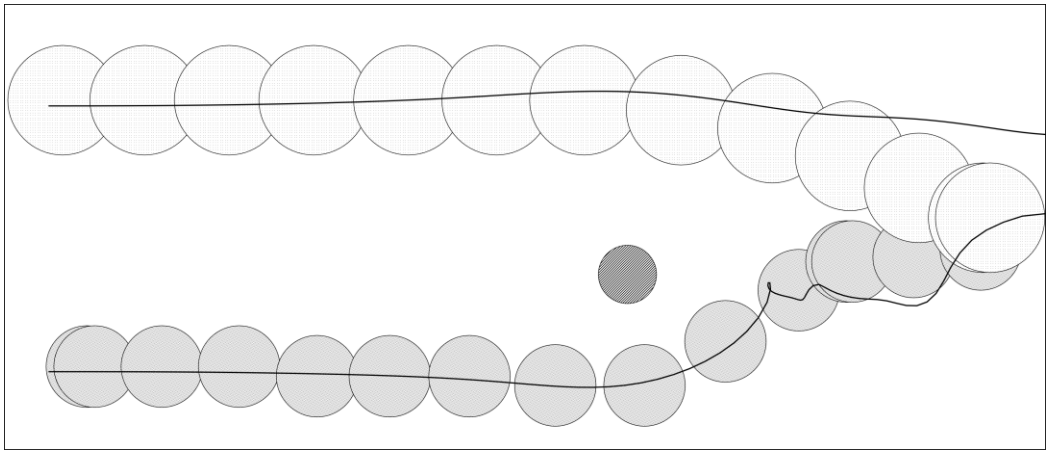

***Fig 3.17**: The image reports the case 1 with a cylinder diameter of 3 mm. The lower particle (white in AutocadMap) has a diameter of 4 mm, it is an example of numerical solution with an heterogeneous velocity field particle*

Conclusions

In this dissertation the interaction mechanisms between cylindrical collectors and particles of different diameters have been studied, a particular relevance assumes the Cheerios effect that is considered as the most relevant responsible of the interactions. The analysis is based on three experimental investigations developed in an artificial flume at the ICEA Department of Padua.

The numerical model elaborated by *Peruzzo et al.* (2013) predicts the trajectories of floating particles subjected to a uniform water flow in proximity of emerging stems, the computation assumes *Re* values lower than 48.

The purpose of this research is to verify if the model describes appropriately the phenomena for *Re* values higher than 48.

After having examined the comparison between numerical and observed paths it is possible to say that the numerical model, in most of cases, guarantees a good approximations of the solutions.

In further researches, to avoid imprecisions, some improvement can be developed. In particular: *i)* a reformulation of the capillary force that considers the actual magnitude for small distances between the particle and collectors can be studied and *ii)* the capillary trapping could be tested in a flume of smaller dimensions to obtain a better uniformity of the velocity and an higher precision in the computation of some parameters.

It could be interesting the study of the trapping with spheres of different materials, if they were of the same weight but with a smaller diameter the mistake in centroid and particle velocity can be reduced.

REFERENCES

- Defina, A., and P. Peruzzo (2010), Floating particle trapping and diffusion in vegetated open channel flow, Water Resour. Res., Vol 46.
- Defina, A., and P. Peruzzo (2012), Diffusion of floating particles in flow through emergent vegetation: Further experimental investigation, Water Resour. Res., 48.
- Defina A., Peruzzo P. and Stocker R., (2013), Capillary Interception of Floating Particles by Surface-Piercing Vegetation, Physical Review Letters, p. 11
- Drazin P.R. (2002), Introduction to hydrodynamic stability, p. 313-315
- Fey U., Konig M., and Eckelmann H., (1998). Strouhal-Reynolds number relationship for the circular cylinder in the range $47 < Re < 2 \cdot 10^5$. Physics Fluids, Vol 10, No. 7, 1547-1549.
- Umeda S., and Yang W-J., (1991). Dynamics of particles floating on liquid flowing in a semicircular open channel, Experiments in Fluids 12, 106-112
- Vella D., and L. Mahadeven (2005). The" Cheerios effect", American Journal of Physics, Vol. 73, 817-825